LIMNOLOGY
and
OCEANOGRAPHY: METHODS

ASLO

Limnol. Oceanogr.: Methods 15, 2017, 847–866

doi: 10.1002/lom3.10204

A coupled metabolic-hydraulic model and calibration scheme for estimating whole-river metabolism during dynamic flow conditions

R. A. Payn [1,2]* R. O. Hall, Jr.,[3] T. A. Kennedy,[4] G. C. Poole,[1,2] L. A. Marshall[5]

[1]Department of Land Resources and Environmental Sciences, Montana State University, Bozeman, MT, USA
[2]Montana Institute on Ecosystems, Montana University System, Bozeman, MT, USA
[3]Department of Zoology and Physiology, University of Wyoming, Laramie, WY, USA
[4]Grand Canyon Monitoring and Research Center, Southwest Biological Science Center, U. S. Geological Survey, Flagstaff, AZ, USA
[5]School of Civil and Environmental Engineering, University of New South Wales, Sydney, New South Wales, Australia

Abstract

Conventional methods for estimating whole-stream metabolic rates from measured dissolved oxygen dynamics do not account for the variation in solute transport times created by dynamic flow conditions. Changes in flow at hourly time scales are common downstream of hydroelectric dams (i.e., hydropeaking), and hydrologic limitations of conventional metabolic models have resulted in a poor understanding of the controls on biological production in these highly managed river ecosystems. To overcome these limitations, we coupled a two-station metabolic model of dissolved oxygen dynamics with a hydrologic river routing model. We designed calibration and parameter estimation tools to infer values for hydrologic and metabolic parameters based on time series of water quality data, achieving the ultimate goal of estimating whole-river gross primary production and ecosystem respiration during dynamic flow conditions. Our case study data for model design and calibration were collected in the tailwater of Glen Canyon Dam (Arizona, U.S.A.), a large hydropower facility where the mean discharge was 325 m^3 s^{-1} and the average daily coefficient of variation of flow was 0.17 (i.e., the hydropeaking index averaged from 2006 to 2016). We demonstrate the coupled model's conceptual consistency with conventional models during steady flow conditions, and illustrate the potential bias in metabolism estimates with conventional models during unsteady flow conditions. This effort contributes an approach to solute transport modeling and parameter estimation that allows study of whole-ecosystem metabolic regimes across a more diverse range of hydrologic conditions commonly encountered in streams and rivers.

Whole-stream metabolism is an integral measure of the link between aquatic and terrestrial ecosystem function (Williamson et al. 2008), and provides insights into the role of river networks in terrestrial carbon cycling and transport (Cole et al. 2007; Hotchkiss et al. 2015). Accurate understanding of the connections between river network and global carbon cycles requires characterization of the controls on whole-river metabolism and gas evasion in diverse environments and hydrologic conditions (Cole et al. 2007; Raymond et al. 2013). However, limitations of conventional methods have prevented study of metabolic processes in rivers that are subject to substantial sub-daily variation in discharge, such as managed flow variation downstream from dams or natural flow variation due to upstream precipitation and evapotranspiration regimes. This lack of information during changing flow conditions may obscure the importance of hydrologic context in our broader understanding of the primary controls on biological production in rivers.

We used hydroelectric flow management on the Colorado River below Glen Canyon Dam (Arizona, U.S.A.) as a case study for development of new whole-river metabolism estimation techniques, specifically for the purpose of overcoming the current limitations in estimating metabolism during dynamic flow conditions. From methodological, scientific, and applied perspectives, flow variations in the tailwaters of hydroelectric dams provide an opportunity to understand river metabolic regimes in the context of unsteady flow. From a methodological perspective, flow regimes are tightly controlled and repeatable, allowing for a predictable pattern in daily flow and a wide range of flow conditions derived from seasonal variation in electrical power demands (Cushman 1985). From a scientific perspective, tailwaters represent

*Correspondence: rpayn@montana.edu

a dramatically altered ecosystem that provides insight into controls on ecosystem function when compared to ecosystems with unaltered flow and sediment regimes (Cushman 1985; Poff et al. 1997). Scientific research is especially illustrative with the opportunity for controlled, large-scale flow manipulation experiments, which also provide data that facilitate development of adaptive management strategies (Bednarek and Hart 2005; Melis et al. 2012). From a management perspective, a dam's tailwater presents widespread challenges to maintaining ecosystem or geomorphological integrity relative to historical conditions before dam construction, such as maintaining a viable habitat and food supply for native endangered species (e.g., humpback chub, *Gila cypha*, in the Colorado River (Melis et al. 2012)) or maintaining historic sedimentary channel structures that facilitate recreational river use (e.g., sand bars for rafters' camp sites (Topping et al. 2010)). In this study, we developed methodology for estimating metabolism that will enable more robust science and more informed management decisions regarding the effect of managed flows on biological production in tailwater aquatic ecosystems.

Estimation of metabolism specific to tailwaters below dams generally requires the two-station technique (Marzolf et al. 1994), which is based on inferring the mechanisms that produce a change in dissolved oxygen (DO) over a river reach rather than the changes in DO at a single location. Use of the two-station technique ensures that the lentic ecosystem in the upstream reservoir does not influence assessment of metabolism specific to the tailwater lotic ecosystem. Most two-station approaches for estimating whole-river metabolic rates of gross primary production (GPP) and ecosystem respiration (ER) stem from the original method in Odum (1956) that assumes DO transport velocities over a reach are uniform over a day of analysis (Marzolf et al. 1994; Hall et al. 2016). Therefore, conventional approaches are likely to provide biased estimates of GPP and ER when this assumption is violated due to changes in flow during a given period of data analysis (typically about 32 h). To remove this bias, we coupled a metabolic model with a dynamic flow routing model to produce simulations of DO fate and transport that do not require an assumption of steady flow. The coupled model allows variation in advection rates predicted by the routing model to affect the duration of time over which advected DO is subject to the metabolic process rates predicted by the metabolic model.

We then developed Bayesian inference methods (Marshall et al. 2004; Smith and Marshall 2008) to estimate river hydraulic properties (friction parameters), metabolic rates (GPP and ER), and physical gas exchange rates with the atmosphere. Time series data required for these inferences included continuous measurements of DO, temperature, and electrical conductivity collected in situ during dynamic flow conditions. These inference schemes contribute methodological advances in both hydrological and biological modeling of rivers. First, we employed a rudimentary particle tracker to develop a simplified, but effective, approach to estimating friction parameters for routing models when water velocity data are limited. Second, we designed an analysis for the metabolic model that relates precision in estimates of physical gas exchange rates to the magnitude of GPP. A better understanding of the drivers of uncertainty in physical gas exchange inferred from DO data is particularly important to confidence in ER estimates (McCutchan et al. 1998).

The coupled model was tested against a conventional two-station river metabolism model with case study data from both unsteady and steady flow periods below Glen Canyon Dam. This test was designed to demonstrate the potential error in metabolism estimates if a conventional steady-flow model is used to estimate metabolism during dynamic flow conditions. Perhaps more importantly, this test was also designed to ensure that the coupled model and conventional models produce the same estimates of metabolism during steady flow conditions. Similar performance during steady flow is critical to confidence that metabolic rates estimated using the coupled model will allow for meaningful comparisons with metabolic rates reported in the literature.

Study site and field data collection

We used our coupled model to assess whole-river ecosystem metabolism for a 12-km reach of the Colorado River located between Glen Canyon Dam and Lees Ferry. The upstream end of the reach was located 14 km downstream from the dam, and the downstream end of the reach was located 0.6 km upstream from the Lees Ferry gage. Flow management for hydroelectric power generation typically results in substantial flow variation in the reach over a given day (i.e., hydropeaking). The hydropeaking index for Glen Canyon was 0.17 from 2006 to 2016 (Kennedy et al. 2016), where the hydropeaking index is defined as the daily coefficient of variation of flow averaged over a period of record (Zimmerman et al. 2010). River discharge originates from release of the hypolimnion in Lake Powell, and thus water temperatures in the study reach are relatively cold throughout the year, with low diel fluctuation. Thalweg temperatures in Glen Canyon typically vary approximately 0.5–1°C over a given day (Hall et al. 2015), with variation in temperature along the reach generally being lower than the total variation within a day (see examples below).

At the mean annual discharge of 325 $m^3 s^{-1}$, average river width is approximately 129 m and average thalweg depth is approximately 4 m along Glen Canyon (Grams et al. 2007). The average bed slope over the study reach is 0.0003 m m^{-1}, and variation in the energy slope includes pools and riffles but does not include any rapids. Channel substrate consists of cobble-gravel bars, talus of variable sizes, and bedrock cliff faces. Pool bottoms and other sandy substrates support rooted vascular macrophytes and branched-form algae

(*Potamogeton* spp. and *Chara* spp.), whereas filamentous green algae (*Cladophora* spp.) and mosses dominate cobble-gravel bar substrates throughout most of the year (Cross et al. 2011). The water is relatively clear for all but a few days of the year due to sediment trapping by Lake Powell and a lack of perennial tributaries between Glen Canyon Dam and Lees Ferry. Generally clear water reduces the potential for light-limitation of photosynthesis associated with dense growth of algae and aquatic plants in the spring and summer.

Model boundary conditions for upstream flows were based on release data for Glen Canyon Dam collected by the US Bureau of Reclamation (http://www.usbr.gov/uc/water/crsp/cs/gcd.html). Calibration data for downstream flows were based on measurements from the USGS stream flow gage at Lees Ferry (station number 09380000). We have been measuring DO concentrations at the upstream and downstream ends of this study reach relatively continuously since March 2008. YSI model 6920 water quality sondes were deployed at the upstream and downstream ends of the reach. Each sonde recorded data at 5-min intervals and was equipped with temperature, electrical conductivity, and dissolved oxygen probes. Monitoring locations were selected by favoring channel structures and equipment placement likely to maximize mixing of thalweg water in the vicinity of the sonde. The upstream sonde was deployed from a large boulder in swift current and the downstream sonde was deployed from a mid-channel navigation buoy. We performed sonde maintenance approximately monthly. During maintenance, we calibrated both sondes simultaneously in a DO-saturated, 80-L metal tub (Hall et al. 2015). Air was bubbled vigorously through water in the tub using an aquaculture pump and air stone, to fully saturate aqueous gas concentrations. The 80-L tub was half immersed in the river during the calibration process to maintain water temperatures similar to the channel. Electrical conductivity was calibrated using a 1000 μS cm^{-1} standard.

Air–water gas exchange rates were estimated using dome experiments within the study reach (Marino and Howarth 1993). Briefly, we used a 10-L metal mixing bowl for a dome that was fitted with two ports, one for the introduction of N_2 gas and one for fitting an oxygen electrode. The edge of the dome was surrounded by PVC plastic to provide flotation. The volume of the headspace enclosed by the dome was 3.95 L and the surface area of water under the dome was 0.064 m^2. We used Orion model 835A oxygen probes that were calibrated using the two-point method (zero and water-saturated air). One oxygen probe measured the air in the headspace of the dome while the second measured the temperature and dissolved oxygen concentration of river water immediately below the dome. At the start of each sampling run, the dome was placed on the river surface while tethered to a boat floating in the current. Nitrogen gas was pumped into the dome until oxygen concentrations in the dome atmosphere were less than 1% of atmospheric saturation concentration. The nitrogen port was then sealed, a piece of moist cloth was draped over the dome to prevent heating of the airspace, and then probes recorded oxygen and temperature in the dome and river water every 5 min while floating downstream with the current. Each dome measurement lasted for 30–60 min. We completed 41 dome experiments that collectively spanned our 12-km study reach during February through March 2004. Dome experiments occurred several years before continuous DO monitoring began in 2008, and data from dome experiments are not available during the same time periods as whole-river gas exchange estimates.

Model development and assessment methods

Model construction

The dynamic flow model was constructed by coupling a dynamic-wave river routing model implemented in an Eulerian finite-element model structure (Walton et al. 1995; Poole et al. 2004) with a metabolic model of oxygen dynamics. The Eulerian reference frame divides a river into a one-dimensional array of stationary compartments, where simulations determine the movement of water and solutes between adjacent compartments and across external boundaries. Boundaries include inputs at the upstream end of the reach and outputs at the downstream end of the reach, as well as conceptual source and sink boundaries along the reach characterizing the processes driving solute dynamics. This approach differs from the more typical implementation of two-station river metabolic models using a Lagrangian reference frame (or perhaps more precisely a quasi- or pseudo-Lagrangian reference frame, *sensu* Ensign et al. (2017)), which is based on simulating dynamics of solutes occurring within mobile parcels of water as they are transported downstream (*see* Doyle and Ensign (2009) or Ensign et al. (2017) for a more thorough comparison of Eulerian and Lagrangian reference frames). The Lagrangian approach originated with the seminal concept for estimating metabolism from changes in oxygen during the travel time between two stations in flowing waters, as developed by Odum (1956). To ensure that differing numerical effects within the two computational approaches did not cause inconsistencies in metabolism estimates, we also implemented a conventional Lagrangian two-station river metabolism model (similar to Hall et al. (2016)) and compared metabolism estimates from the Eulerian and Lagrangian models using the same DO data from steady flow conditions.

Despite differences in computational approach, the conceptual treatment of oxygen mass balance in the two model structures is consistent with the fundamentals of most conventional stream metabolism models. Both models incorporate the same four controls on DO concentration: gross primary production, ecosystem respiration, physical exchange with the atmosphere, and downstream advection

in the river channel (i.e., the basic processes defined by Odum (1956) and the foundation of most subsequent models). Thus, the only differences between the models are in their computational reference frames and whether or not they simulate the influence of unsteady flow.

Formulations for metabolism and atmospheric exchange of DO

For both the Eulerian dynamic flow model and the Lagrangian steady flow model, the same basic equations were the basis for calculations of DO fluxes due to metabolism and exchange with the atmosphere. We assumed instantaneous gross primary production (P_{GPP}, g O_2 m^{-2} s^{-1}) was proportional to the shortwave radiant energy (or photosynthetically active radiation, PAR) available for photosynthesis (E_{PAR}, μmol-photons m^{-2} s^{-1}).

$$P_{GPP} = \alpha_{GPP} E_{PAR} \quad (1)$$

where α_{GPP} is the proportionality constant for GPP vs. radiation (g-O_2 μmol-photons^{-1}). The model parameter α_{GPP} was estimated using Bayesian inference with both models (see details below), and was assumed to be time invariant over a given 32-h dataset (22:00 until 06:00) used for the inference. After estimation of α_{GPP}, the daily average gross primary production ($\bar{P}_{GPP}$, g O_2 m^{-2} d^{-1}) was calculated from the integral of E_{PAR} throughout the time period used for inference.

$$\bar{P}_{GPP} = \frac{\alpha_{GPP} \int_{t_0}^{t_{end}} E_{PAR} dt}{1 \text{ day}} \quad (2)$$

where t_0 is the start time of the analysis (s) and t_{end} is the end time of the analysis (s). Studies have suggested that the relationship of E_{PAR} radiation and P_{GPP} is likely to reflect a saturating asymptotic increase to a maximum primary production rate (e.g., hyperbolic or Michaelis–Menten equation (Holtgrieve et al. 2010)), though the simple linear model may be sufficient in some locations or in the context of other sources of error (Mulholland et al. 2001; Hall et al. 2016). We chose to use the simpler one-parameter linear model for parsimony, and we will adapt the formulation if GPP is demonstrated to saturate at high PAR levels in this ecosystem and the available DO data provide sufficient information for a more complex two-parameter model.

We assumed inputs for E_{PAR} to be longitudinally uniform along the canyon and vary through time based on theoretical calculations that account for the averaged effect of shading from the canyon walls (Yard et al. 2005). These driving E_{PAR} data do not currently account for the influence of spatial variation in shading along Glen Canyon or temporal variation in PAR due to cloud cover. Therefore, we do not interpret values of α_{GPP} as the "true" relationship between primary production and radiation incident on the water surface. In this case, estimates of α_{GPP} are used only to ensure that the normalized temporal distribution of P_{GPP} is identical to the theoretical normalized distribution of E_{PAR} over a given day of analysis.

The parameter for instantaneous ecosystem respiration (R_{ER}, g O_2 m^{-2} s^{-1}) was estimated using Bayesian inference with both models (*see* details below), and was assumed to be time invariant within a given 32-h dataset (22:00 until 06:00) used for the inference. Therefore, daily mean ecosystem respiration ($\bar{R}_{ER}$, g O_2 m^{-2} d^{-1}) was calculated from R_{ER} using simple unit conversion. We use a negative sign convention for respiration ($R_{ER} \leq 0$) because respiration always removes DO from the channel water mass balance. Assumption of uniform R_{ER} over a day is clearly not an accurate representation of real ecosystems (Tobias et al. 2007; Hotchkiss and Hall 2014) and may cause bias in estimates of both GPP and ER. However, rigorous exploration of diel variation in R_{ER} without further assumptions requires additional data that were not available for our site (e.g., oxygen isotope data (Holtgrieve et al. 2010)), so we chose the simpler model for initial model development.

Movement of oxygen across the air–water interface at the river surface is governed by the average saturation deficit of DO in river water (C_{OD}, g O_2 m^{-3} used in model calculations for all DO concentrations).

$$C_{OD} = C_{OS} - C_O \quad (3)$$

where C_{OS} is the temperature- and pressure-dependent saturation concentration of DO in water and C_O is the concentration of DO in river water. Values of C_{OS} were calculated using theoretical relationships with water temperature, water density, and atmospheric pressure (García and Gordon 1992) (*see* Appendix).

The rate of oxygen movement between the river and atmosphere was calculated from the gas exchange velocity k (m s^{-1}).

$$J_O = k C_{OD} \quad (4)$$

where J_O is the mass flux of oxygen across the water surface (g O_2 m^{-2} s^{-1}). Positive J_O values increase simulated DO concentration, and negative J_O values decrease simulated DO concentration. We accounted for variation in k with temperature based on the theoretical dimensionless Schmidt number for oxygen in water (*see* Appendix), thus yielding the model parameter k_{600} (the gas exchange velocity at a Schmidt number of 600) as the primary modeled control on physical air–water gas exchange. The k_{600} parameter was estimated using Bayesian inference with the Eulerian dynamic flow model (see details below), and was assumed to be time invariant over a given 32-h dataset (22:00 until 06:00) for both models.

Lagrangian steady flow DO model

We conceptualized a representative parcel of water traveling our study reach in a Lagrangian reference frame by defining a starting DO concentration at the upstream end of the

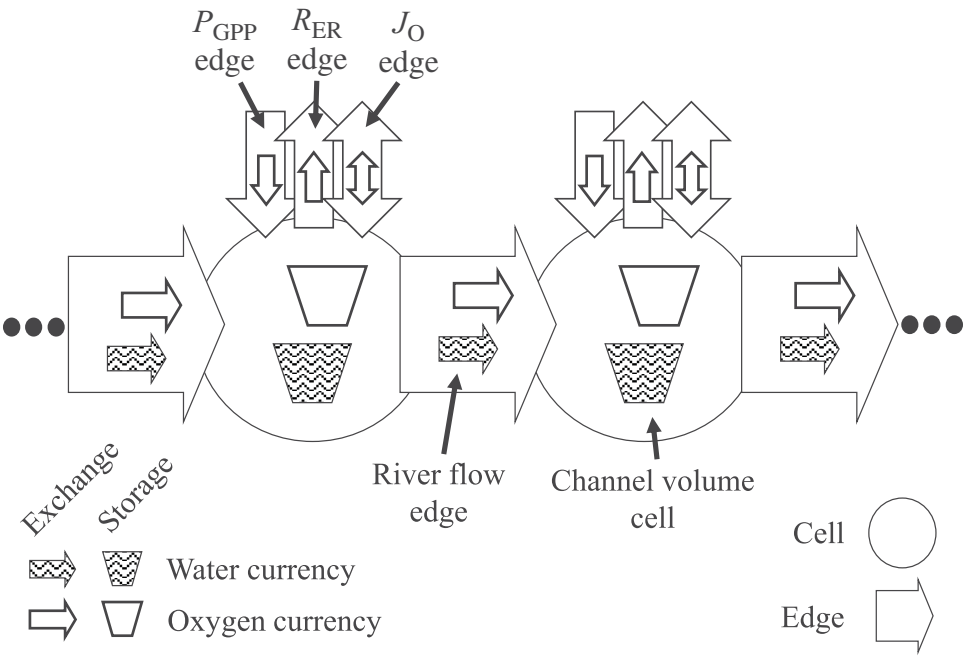

Fig. 1. Conceptual diagram of the Eulerian dynamic flow model, as implemented with coupled river routing and dissolved oxygen models within the Network Exchange Objects framework. Sequence of channel cells, flow edges, and ellipses symbols (...) indicate the repeated pattern used to simulate a one-dimensional river flow and metabolic system. Gross primary production (P_{GPP}), ecosystem respiration (R_{ER}), and physical air–water exchange (J_O) edges contain modules that use the associated equations to simulate introduction or removal of oxygen from dissolution in the associated channel water cell (based on the α_{GPP}, R_{ER}, and k_{600} parameters, respectively).

reach as C_{O,t_U}, where t_U (s) denotes the time the parcel passed the upstream measurement location. Following the same parcel of water, we defined its DO concentration at the downstream end of the study reach as $C_{O,t_U+\bar{t}_R}$, where $\bar{t}_R$ (s) is the average travel time of water in the reach. We then mathematically defined the change in DO concentration between the upstream and downstream ends of the reach, based on the components of DO mass balance as described above.

$$C_{O,t_U+\bar{t}_R} - C_{O,t_U} = \frac{1}{\bar{z}}\left(\alpha_{GPP}\int_{t_U}^{t_U+\bar{t}_R} E_{PAR}dt + R_{ER}\bar{t}_R + k\bar{t}_R\frac{C_{OD,t_U}+C_{OD,t_U+\bar{t}_R}}{2}\right) \quad (5)$$

where $\bar{z}$ is the average depth of river water over the reach (m), C_{OD,t_U} is the oxygen saturation deficit at the upstream end of the reach at time t_U, and $C_{OD,t_U+\bar{t}_R}$ is the oxygen saturation deficit at the downstream end of the reach at time $t_U+\bar{t}_R$. After substituting $C_{OS,t_U+\bar{t}_R}-C_{O,t_U+\bar{t}_R}$ for $C_{OD,t_U+\bar{t}_R}$ based on Eq. 3, Eq. 5 was algebraically rearranged to isolate $C_{O,t_U+\bar{t}_R}$ on one side and thus provide an explicit Lagrangian model of the downstream DO concentration as a function of upstream concentration.

$$C_{O,t_U+\bar{t}_R} = \frac{C_{O,t_U} + \frac{1}{\bar{z}}\left(\alpha_{GPP}\int_{t_U}^{t_U+\bar{t}_R} E_{PAR}dt + R_{ER}\bar{t}_R + k\bar{t}_R\frac{C_{OD,t_U}+C_{OS,t_U+\bar{t}_R}}{2}\right)}{1+\frac{k\bar{t}_R}{2\bar{z}}} \quad (6)$$

This model can only accurately simulate DO dynamics during steady flow conditions, because $\bar{z}$ and $\bar{t}_R$ are hydrologic parameters that are held constant during a day of analysis. The value of the gas exchange velocity k in Eq. 6 was calculated as a function of the parameter k_{600} (*see* Appendix), based on the average temperature of the parcel of water during its travel time over the reach ($\bar{T}=0.5\left(T_{t_U}+T_{t_U+\bar{t}_R}\right)$). The remaining parameters for this model are α_{GPP} and R_{ER}, which control the magnitude of the effects of GPP and ER on DO concentrations.

Eulerian dynamic flow coupled model

We constructed the channel water routing model based on an existing dynamic surface flow model using the Network Exchange Objects (NEO) framework (Fig. 1). NEO is a highly modular and extensible object-oriented framework for facilitating the numerical simulation of the interactions of "currencies" in distributed exchange networks (Izurieta et al. 2012). In this case, the exchange network of interest is a one-dimensional river channel, and the two currencies of interest are the water and DO in that channel. The hydrologic component of the model was adapted from an existing implementation of the water currency from the Water and Resource Exchange Network (WREN) model (e.g., Helton et al. 2014), which was based on a modified version (Poole et al. 2004) of the Wetland Dynamics Water Budget Model (Walton et al. 1995). The WREN water currency includes a dynamic-wave routing module for surface water, and thus

simulates the movement of both water (solute pulse) and mechanical energy (flood wave pulse) along the river channel. We developed the DO currency to depend on flows and volumes predicted by the water currency, in order to simulate DO advection and concentrations along the channel. The NEO framework is specifically designed to facilitate this type of currency interaction, because the objects constituting a given currency model can directly access the objects constituting a different currency model located in the same location within the shared model structure (i.e., objects from multiple currencies share the same namespace structure). Additional modules of the DO currency were implemented to simulate the influence of primary production (based on Eq. 2), respiration (based on parameter R_{ER}), and atmospheric exchange (based on Eqs. 3, 4) on the mass balance of DO in channel water. These processes were simulated as rates of exchange with source or sink boundary conditions along the channel (Fig. 1).

The abstraction of a distributed exchange network in a NEO model consists of *cells* that store currencies and *edges* that move quantities of currencies between a given pair of adjacent cells (Izurieta et al. 2012). We conceptualized our 12-km long study reach within this abstraction as a one-dimensional series of 120 consecutively adjacent cells, where each cell represents a 100-m sub-reach of the river channel that stores a finite volume of water and a finite mass of DO (Fig. 1). We then implemented objects in edges that simulate river flow and oxygen transport along the channel as a series of water and DO exchanges between adjacent pairs of river cells, hence the one-dimensional Eulerian reference frame. The model was typically run at a 5-s time step, but would sometimes require a shorter time step for stability at the highest flows. As with all finite difference models, discretization of space and time in these simulations were a compromise between model stability, accuracy, and runtime.

The NEO framework automatically performs a mass balance for a given currency in each cell by summing the influences of the exchanges of that currency with adjacent cells during each time step. Therefore, the effective finite difference calculation of the mass balance of water in a given cell of the one-dimensional river network was defined as

$$V_{t+\Delta t} = V_t + \Delta t Q_{E,U} - \Delta t Q_{E,D} \quad (7)$$

where V_t and $V_{t+\Delta t}$ are the volume of water (m^3) in the cell before and after a model time step Δt (s), and $Q_{E,U}$ and $Q_{E,D}$ are the exchange of water (i.e., downstream flow, $m^3\ s^{-1}$) with the adjacent cells in the upstream (input) and downstream (output) directions, respectively.

Simulations of $Q_{E,U}$ and $Q_{E,D}$ in edges along the channel are based on the conservation of momentum from the St. Venant Equations. We used a finite difference approximation of the full dynamic wave equation.

$$Q_{t+\Delta t} = \frac{Q_t + 2u(A_{t+\Delta t} - A_t) + \Delta t u^2 \frac{A_{t+\Delta t}}{R}\left(S_0 - \frac{\Delta H}{\Delta x}\right) + \Delta t g A_{t+\Delta t}\frac{\Delta H}{\Delta x}}{1 + \frac{\Delta t g n^2 u}{R^{4/3}}} \quad (8)$$

where Q_t and $Q_{t+\Delta t}$ are the volumetric flow of water ($m^3\ s^{-1}$) in an edge at the beginning and end of a model time step, g is acceleration due to gravity ($m\ s^{-2}$), A_t and $A_{t+\Delta t}$ are the cross-sectional area of the wetted channel (m^2) at the beginning and end of a model time step, $\Delta H/\Delta x$ is the hydraulic gradient along the edge, S_0 is the average bed slope between the adjacent cells, n is Manning's roughness coefficient (assuming SI units), u is the depth-averaged velocity of water between cells ($m\ s^{-1}$), and R is the hydraulic radius of the wetted channel (m). This formulation from the Wetland Dynamics Water Budget model (Walton et al. 1995) is similar to the formulation used in the EPA Storm Water Management Model (Rossman 2006). We assumed a rectangular channel cross-section with uniform bed slope for each model cell, resulting in a constant width and a cross-sectional area that varied proportionally with depth. Bed slope S_0 was 0.0003 $m\ m^{-1}$ and channel width was 129 m, based on reach-averaged data from morphological studies in Glen Canyon (Grams et al. 2007).

We adopted the general form of the function characterizing the empirical nonlinear relationship between river depth and bed friction used by Wiele and Smith (1996), but we recalibrated the parameters of the function to be more specific for flow in Glen Canyon. For a given exchange between cells, the ratio of local depth-average water velocity to shear velocity (u^*) was assumed to increase linearly with the log-transform of the hydraulic radius (a convex, non-linear increase of u/u^* with increasing R), which has been demonstrated to be applicable to flow in the Grand Canyon region of the Colorado River (Wiele and Smith 1996).

$$\frac{u}{u^*} = f_b + f_m \ln R \quad (9)$$

where f_b and f_m are model parameters representing the intercept and logarithmic slope of the empirical friction-depth relationship. Values for parameters f_b and f_m were calibrated using Bayesian inference and considered invariant in time and space. A time variant Manning's n (for use in Eq. 8) was subsequently calculated for a given exchange between cells, based on the ratio of depth-average velocity to shear velocity (Wiele and Smith 1996).

$$n^2 = \frac{R^{1/3}}{\left(u/u^*\right)^2 g} \quad (10)$$

Input data (e.g., from dam release data or calibrated simulations) provided the upstream flow boundary condition, and the downstream flow boundary condition was based on the assumption that the hydraulic gradient at the model outflow is approximately equal to the hydraulic gradient between

the last two cells. This assumption is invalid at times when flow is changing rapidly. Therefore, all models included at least 1 km of additional simulated channel between the downstream end of the study reach and the downstream model boundary, which minimized the potential for transient inaccuracies in the downstream boundary conditions to influence the simulated study reach.

A rudimentary agent-based particle tracker was implemented within the hydrologic model to simulate reach average travel times. The particle tracker releases particle agents at the upstream end of the simulated reach at a user defined rate, and tracks the average travel time since release reported by the particle agents after they have arrived at a user defined downstream edge. During a simulation, the particle agents move through consecutive edges in the network at a rate equal to the value of u (depth average velocity or Q/A) in each edge, and individually track the passage of simulated transport time since their release.

The dissolved oxygen currency was coupled to the water currency through the shared state space within the channel cells and edges defined in the NEO framework (Fig. 1). In this way, the simulation of the mass balance of oxygen in each channel cell is effectively calculated based on water movement (Eq. 8) along with the influence of metabolic activity and gas exchange with the atmosphere (Eqs. 1, 4).

$$M_{O,t+\Delta t}=M_{O,t}+\Delta t Q_{E,U}C_{O,U}-\Delta t Q_{E,D}C_O+A_{WS}(P_{GPP}+R_{ER}+J_O) \tag{11}$$

where $M_{O,t}$ and $M_{O,t+\Delta t}$ are the mass of oxygen (g) in the cell before and after a model time step, C_O is the concentration of oxygen in the cell, $C_{O,U}$ is the concentration of oxygen in the next cell upstream, and A_{WS} is the wetted surface area of the channel cell (in this case, a constant 12,900 m^2). This equation does not include the potential influence of solute transport via longitudinal dispersion or transient storage, which could lead to bias in metabolism estimates (Hensley and Cohen 2016). Our initial development was focused on determining model consistency with conventional models, and metabolism models that include the influence of dispersion are a relatively recent development. However, the modularity of our dynamic flow model is particularly well-suited to numerical experiments with alternative formulations, and assessing the influence of simulated dispersion on metabolism estimates is a potential direction for future research. The value of P_{GPP} is always ≥ 0 and is calculated in a cell boundary as a function of PAR input as described by Eq. 1. The value of R_{ER} is always ≤ 0 and is a direct model input parameter. The value of J_O can be positive or negative (depending on DO concentration relative to saturation) and is calculated in a cell boundary as described in Eq. 4. For calculation of J_O, DO saturation and temperature are based on the average of the upstream and downstream temperature during a given model iteration. This assumption is not likely to be an accurate estimate in rivers with large temperature fluctuations. However, as mentioned above, thalweg water temperatures vary little along our study reach.

Model calibration and parameter estimation

All parameter estimates were random variables characterized by posterior probability distributions from Bayesian inference. Simulations of posteriors were based on Markov Chain Monte Carlo (MCMC) sampling from proposed parameter sets, using the Adaptive Metropolis proposal algorithm for faster convergence. Code for parameter estimation schemes was developed in Java (Oracle Corporation, Redwood Shores, California, U.S.A.) and adapted from algorithms developed for watershed hydrologic studies (Marshall et al. 2004; Smith and Marshall 2008). Decisions to accept or reject proposed parameter sets were based on comparisons of a Bayesian posterior probability that combines a log-likelihood function for observations conditional on parameters and the prior probability of those parameters.

$$\ln\left[P(\theta|D_O)\right] \propto \sum_i \ln\left[P(\theta_i)\right]-\frac{1}{2\sigma^2}\sum_{j=1}^{n}\left(d_{P,j}-d_{O,j}\right)^2-\frac{n}{2}\ln\left(2\pi\sigma^2\right) \tag{12}$$

where D_O is an observed data set from which model parameters are being inferred, θ is a proposed set of values for the inferred parameters, $P(\theta|D_O)$ is the posterior probability for a given θ, $P(\theta_i)$ is the prior probability for the i th parameter value in θ, $d_{O,j}$ is the j th observation in D_O, $d_{P,j}$ is the model prediction corresponding to $d_{O,j}$, σ^2 is the variance of normally distributed residual errors (i.e., $d_{P,j}-d_{O,j}$), and n is the total number of observations being compared to model predictions. Equation 12 includes the implicit assumption that all sources of error are included in a single, normal distribution defined by σ^2, and that elements of that distribution are independent and homoscedastic. Structure in the residual errors from our highest posterior probability parameter sets suggest that these assumptions were often violated due to temporal autocorrelation. Autocorrelation in error is seldom addressed in metabolic inference schemes in rivers, and exploration of the potential bias in parameter estimates or uncertainty introduced by neglecting temporal autocorrelation will be an important area of future study to improve statistical rigor. We would expect that a failure to account for autocorrelation in residual error generally leads to artificially narrow confidence intervals on parameter estimates.

Estimation of model parameters was conducted with two independent model fitting exercises, first with the hydrologic model alone and then with the coupled metabolic model. The hydrologic model was first fit to discharge and velocity data to estimate values for parameters controlling channel friction calculations (f_b and f_m). The metabolic model was subsequently fit to DO data over 32-h time

periods to estimate values for parameters controlling GPP, ER, and gas exchange calculations (α_{GPP}, R_{ER}, and k_{600}).

Uniform prior distributions with bounds extending beyond conceivable values were used in calculating posterior probabilities (Eq. 12) for all parameters except k_{600}. Posterior distributions resulting from Bayesian inference were generally not stacked against the bounds of the prior distributions, unless observation data exhibited physically unlikely patterns or were obviously subject to substantial drift. Therefore, we only pursued definition of a more informed prior probability distribution for the k_{600} parameter relative to its problematic interactions with the R_{ER} parameter, and leave derivation of more effective non-uniform prior probability distributions for other parameters to future work (if necessary). Estimation schemes for all parameters, including the derivation of the prior distribution for k_{600}, are described in more detail below.

Hydrologic calibration

The Eulerian dynamic flow model required estimation of friction parameters (f_b and f_m, Eq. 9) that appropriately represent the hydraulics of the Glen Canyon reach of the Colorado River. Previous calibrations of models have provided uniform estimates of these friction parameters aggregated over the entire Grand Canyon segment (Wiele and Smith 1996), but re-calibration for the specific geomorphic structure of Glen Canyon was necessary for our smaller-scale models.

Calibration of a dynamic flow model requires river flow data as well as reach average water velocity data. Upstream river flow data were provided by Glen Canyon Dam release records, and downstream data were provided by the real-time U. S. Geological Survey gage at Lees Ferry. Continuous flow data were readily available, but continuous reach average velocity data were not. Estimates of reach average velocity were available when sharp peaks or troughs were observed in the naturally occurring temporal variation of electrical conductivity. We assumed that the time difference between the arrivals of a given peak or trough at the upstream and downstream end of the study reach was primarily determined by reach average advective transport of total dissolved solids. Applying this logic to multiple flow conditions, we estimated reach average velocity from travel times of water traveling our study reach during discharges ranging from ca. 210 $m^3 s^{-1}$ to 740 $m^3 s^{-1}$ at the Lees Ferry gauge. To maximize the range of flow conditions considered in this calibration, we collected 149 pairings of discharge and velocity from different flow conditions over multiple years of dam operations.

Travel time data were temporally discontinuous across multiple years, so we could not calibrate the hydrologic model based on direct comparisons of simulations to continuous time series data. Therefore, we used a more synthetic strategy of calibrating the model to the observed bivariate relationship between river discharge at Lees Ferry and reach average transport time. A synthetic input for the upstream boundary conditions was created to simulate an increase in flow from 210 $m^3 s^{-1}$ to 740 $m^3 s^{-1}$ over 7 d. The relatively slow simulated change in flow minimized the influence of previous flow states on the reach average transport time of water parcels arriving at the downstream end of the reach (i.e., minimized hysteretic behavior in the discharge vs. transport time relationship). The particle tracker in the model was configured to allow simulations of the decrease in reach average transport times (or increase in reach average velocities) as the upstream discharge boundary condition was increasing. Finally, the MCMC calibration scheme was used with this synthetic model to estimate friction parameters that provided the best fit between the simulated and observed relationships between discharge and travel time. Hydrologic calibration was carried out only once, and independently of the later estimation of metabolic parameters.

Changes in flow in Glen Canyon occurred much faster than simulated change in flow in the calibration exercise, thus hysteretic behavior in reach average velocities with change in discharge was likely in the observed data. For a given discharge, observed reach average travel times on a falling limb were likely to be less than observed reach average travel times on a rising limb. We assumed we had approximately equal sampling on both sides of the hysteresis in the travel time observations. Thus, during calibration, we assumed that fitting a non-hysteretic simulation to hysteretic observations would still effectively approximate the true friction characteristics with minimal bias. To verify the validity of this assumption, we compared the magnitude of residual errors from the model fit to the magnitude of simulated hystereses from calibrated model runs with realistic flow inputs. This comparison allowed us to ensure that the simulated hystereses based on estimated parameters were a reasonable approximation of real hystereses that would be a primary contributor to error in the synthetic model fit.

Metabolic parameter estimation

Estimation of parameters for the metabolic model was based on direct application of a Bayesian inference scheme to the observed and simulated time series of downstream DO concentrations. Estimated parameters included the ratio of PAR and GPP (α_{GPP}, Eq. 1), ecosystem respiration (R_{ER}, Eqs. 6, 11), and the gas exchange velocity (k_{600}). Parameter estimates were carried out on a daily basis, where simulations were compared to observations over a 32 h period for each day and surrounding nighttime periods (22:00 on day 1 through 06:00 on day 3). Based on these parameter estimates, daily average GPP and ER were calculated as described previously.

We wished to set a minimum threshold of uncertainty in metabolic parameter estimates based on the measurement accuracy of our multi-parameter sondes, while maintaining a

relatively simple model of error in the likelihood function that does not distinguish among aleatoric error (e.g., random error), epistemic measurement error (e.g., instrument drift), and epistemic structural error (e.g., missing or inappropriate processes in the model). To prevent unrealistically low uncertainty in parameter estimates, we assumed a fixed value for σ^2 in the likelihood function, rather than the conventional practice of estimating the value of σ^2 with the MCMC algorithm. We chose 0.05 g m^{-3} for the fixed value of σ, based on estimates of the DO measurement accuracy provided with the sondes. Fixing σ to this value prevented unrealistically narrow posterior distributions of parameter estimates from a given exceptionally good model fit, despite known sources of epistemic measurement error in the observed data that are much larger than the residual errors evident from that fit. Our approach still does not address the potential influence of epistemic structural error, but structural uncertainty cannot be easily addressed with the error term in the likelihood function, alone.

Ambiguity in parameter estimates due to model equifinality is likely when attempting to infer both respiration and physical gas exchange rates from a DO time series. The resulting lack of precision in physical gas exchange rates thus inherently leads to higher uncertainty in estimates of ER relative to estimates of GPP (McCutchan et al. 1998). The parameters R_{ER} and k_{600} have strong interdependencies in inferences from metabolic models (i.e., parameter interactions), because increasing or decreasing these parameters can have similar effects on the downstream DO dynamics predicted by the model (i.e., model equifinality) in certain situations. Therefore, confidence in estimates of R_{ER} is strongly aided by independent estimates of k_{600}, typically obtained via gas tracer tests. Whole-system artificial gas tracer tests are not practical in rivers the size of the Colorado, so independent estimates of the effective k_{600} are problematic in our case study. Multiple point measurements of air–water gas exchange were collected using floating domes in 2004, summarized by a normal distribution with a mean of 0.119 m h^{-1} and a standard deviation of 0.013 m h^{-1} (n=41). However, before using these localized measurements to inform our reach simulations, we sought further independent evidence that these point measurements were applicable to whole-reach gas exchange behavior.

Our strategy to mitigate the potential for equifinality in the metabolic model was to establish a more informative Bayesian prior probability distribution for the whole-stream k_{600} model parameter, in the absence of a direct measurement of whole-stream gas exchange rates. To establish this prior probability distribution, daily estimates of k_{600} (along with α_{GPP} and R_{ER}) were inferred using uniform prior distributions in parameter estimates over a period of strongly increasing GPP in the late winter and spring of 2009. Results indicated that higher rates of GPP led to higher precision in k_{600} estimates. This pattern is a consequence of the increase in independent information about k_{600} that is available when diel variation in DO concentration is increased, driving higher variation in the DO saturation deficit. Higher variation in the saturation deficit causes more sub-daily variation in gas exchange with the atmosphere, which creates a pattern in DO data that is more separable from the (assumed) constant influence of ER. Therefore, higher GPP ultimately amplifies the differences between the effect of gas exchange and the effect of ER on DO concentrations. More pronounced differences in the effect of gas exchange and ER subsequently lead to a DO signal that allows more confidence in independent inferences of k_{600} and R_{ER} parameter values. Note that this logic is based on the assumption that R_{ER} is time invariant over a given day of analysis. The additional parameters associated with introduction of diel variation in ER to the model could result in confounded parameter inferences from DO concentration data alone, regardless of high or low GPP rates. As noted above, assessment of bias in metabolism estimates due to sub-daily variation in ER was outside the scope of this project, and requires a substantial amount of additional research.

We exploited the effects of GPP on k_{600} estimates to establish prior information for k_{600} in Glen Canyon. We selected a minimum threshold in GPP, above which estimates of k_{600} could be more precisely inferred from the DO data (Fig. 4b). We fit a normal distribution to the resulting collection of k_{600} estimates with higher certainty, which we subsequently used to describe the prior probability for estimation of k_{600} in following analyses. We compared this distribution derived from the model to the independent distribution based on dome experiments, which tests whether the estimated rates were physically reasonable and if the dome measurements are potentially scalable to whole reach behavior in future work. Dome measurements were used as an independent comparison with the estimated whole-river gas exchange rates, and were not used for derivation of the prior distribution.

Our model does not currently address the bias in metabolism estimates due to potential for sub-daily variation in k_{600} related to dynamic flow conditions. In general, sub-daily variation in gas exchange potential is seldom considered in modeling exercises, regardless of whether the mechanism behind the variation is related to flow or weather. In Glen Canyon, we have the advantage of consistently flat water (deep water relative to substrate size), and the variation in surface turbulence with change in flow is not likely to be as pronounced as that which would occur in shallower rivers. Strong sub-daily variation in gas exchange in Glen Canyon is more likely driven by the typical diel variation in wind. However, we acknowledge that temporal variation in gas exchange potential may be a consequence of variation in flow that is important for more general applications of this approach, and thus assessing the sensitivity of metabolism

estimates to diel variation in k_{600} for any reason may be an important direction for future research.

Comparison of dynamic and steady flow models

Metabolic estimates from the Eulerian dynamic flow model were compared to the conventional Lagrangian steady flow model, which allowed us to: (1) assess if the fundamental differences in model reference frame (i.e., Lagrangian vs. Eulerian) influenced metabolism estimates on a day of steady flow, and (2) assess how assumption of steady flow affects estimates of metabolic rates on a day with substantial variation in flow. These comparisons were based on four independent estimates of α_{GPP} and R_{ER} using both the Lagrangian steady flow model and the Eulerian dynamic flow model. Each model was independently fit to: (1) a day of data with steady flow conditions (345 m^3 s^{-1}, 19 October 2008) during an experimental period of constant-flow dam operations and (2) a day of data with particularly unsteady flow conditions (range of 246–468 m^3 s^{-1}, 20 August 2010) due to higher hydropower demands in the late summer. The models are based on the same physical and biological assumptions about DO processing; therefore, we expect any differences in parameter estimates during steady flow conditions would be attributable solely to the differences in the model reference frames.

For the simulations on the day with unsteady flow, the velocity and depth parameters of the Lagrangian steady flow model were set to the daily average velocity and depth, as simulated by the unsteady flow model at the downstream end of the study reach. To minimize the potential for confounded comparisons due to ambiguous parameter estimates, the parameter k_{600} was held at a fixed value for these comparisons. The same value of k_{600} was used for both models for a given day of analysis, and that value was based on an initial estimate from the dynamic flow model for that day.

Assessment of model performance

We assessed the results of the modeling efforts first in terms of the hydrologic model alone, then in terms of the coupled metabolic model. Our assessment of the coupled model includes the results of developing a prior probability distribution for the k_{600} parameter. Finally, we compared Eulerian dynamic flow model parameter estimates and Lagrangian steady flow model parameter estimates during two time periods of contrasting flow regimes: one with relatively steady flow during a period of experimental control, and one with strong diel flow variation due to hydroelectric power generation, also known as "hydropeaking."

Hydrologic calibration

Calibrated friction parameter values for the hydrologic model ($f_b = -14.81$ and $f_m = 11.90$) were provided by a fit to bivariate discharge and reach average velocity observations (Fig. 2). A meaningful metric of fit or estimate of error was not possible with the abstracted hydrologic calibration scheme applied here. In this case, the posterior distributions do not provide directly useful information about hydrologic accuracy due to assumed hysteretic behavior in the observations. Therefore, the number of significant digits reported here prevented numerical rounding errors in subsequent simulations with the coupled metabolic model, and are not an indication of confidence in parameter estimates.

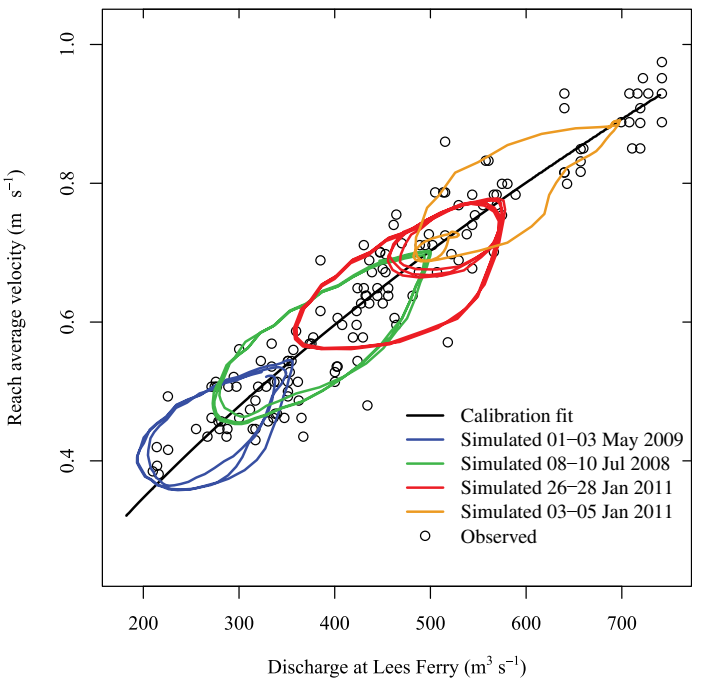

Fig. 2. Observed bivariate relationship between discharge and reach average velocity (circles) and the highest posterior probability simulated relationship between reach average velocity and discharge at Lees Ferry (solid black line). The calibration fit was determined from simulations with a slowly-changing synthetic flow regime that minimized any hysteretic effects on reach averaged velocity. Examples of hystereses in simulations with the calibrated model are presented for real data collected during diel flow regimes spanning the range of flows used for the calibration (blue, green, red, and orange lines).

Substantial residual error around the calibration fit was likely due to hysteretic behavior of reach average velocity relative to hydropeaking flows. For a given instantaneous river discharge condition, reach average velocities will be higher if the discharge trend is decreasing with time (i.e., velocities over the reach were previously faster), compared to the reach average velocities when the discharge trend is increasing with time (i.e., velocities over the reach were previously slower). The hystereses predicted by the calibrated model driven with realistic discharge variations was comparable in magnitude to the residual error around the calibration fit (Fig. 2).

The performance of the hydrologic model calibration was assessed more directly using comparisons between simulations and discharge time series data. Based on a model of the reach from Glen Canyon Dam to Lees Ferry, the predicted

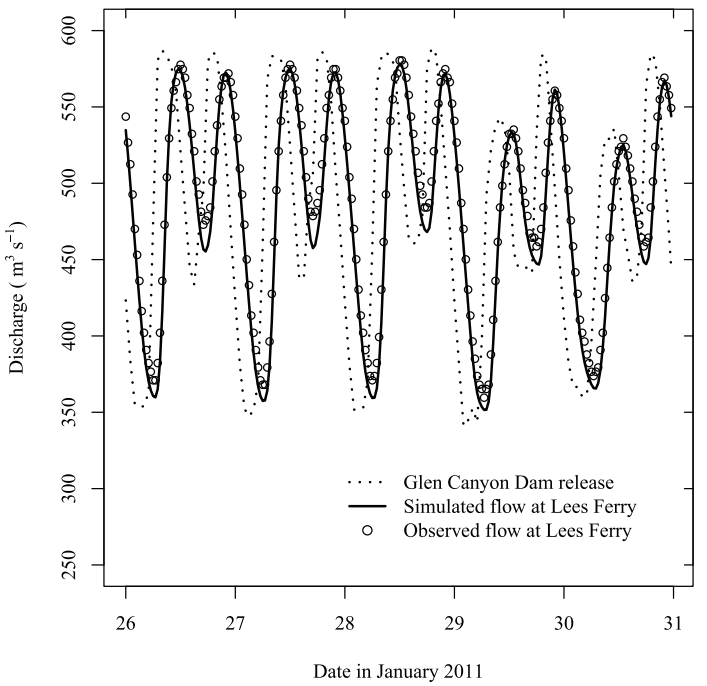

Fig. 3. Hydrographs for the Glen Canyon Dam release (dotted lines), observed flow at Lees Ferry (open circles), and calibrated simulated flow at Lees Ferry (solid lines) for 26 January 2011–30 January 2011 (*see* Fig. 2).

timing of flood pulse arrivals was remarkably accurate (Fig. 3), considering that the model was not directly calibrated to the Lees Ferry hydrograph time series. During select time periods (including the example in Fig. 3), there appeared to be a relatively minor uniform offset between the predicted and observed discharges at Lees Ferry. An offset indicates either an unaccounted water gain or loss along the reach, or a minor inaccuracy in the dam release or flow gage data. We do not expect any of the observed offsets to have a meaningful effect on predicted water velocities; hence, we do not expect this to be a major source of error in the metabolic model parameter estimates.

Prior distribution for k_{600} and metabolic parameter estimates

Based on Bayesian estimation from winter and spring of 2009, the widths of k_{600} posterior distributions generally decreased with the increase in GPP (Fig. 4). This finding suggests that higher $\bar{P}_{GPP}$ resulted in higher precision in k_{600} estimates when no prior information was assumed. We chose a minimum threshold of 5 g O_2 m^{-2} d^{-1}, above which an increase in $\bar{P}_{GPP}$ values provided little improvement in the precision in k_{600} estimates (Fig. 4b). A few estimates from days with higher GPP exhibited unrealistic values for k_{600}, likely due to localized measurement inaccuracies or days with conditions inconsistent with model structure (e.g., variable cloud cover or heavy storms). To avoid using data from days when our model was poorly equipped to estimate metabolic and gas exchange parameters, we chose to restrict our derivation of a prior distribution for $k_{600}$to reasonable values as defined in the range of 0.1–0.25 m h^{-1}. This decision affected the distribution primarily on the high end, as it excluded three outlying data points that were far above the typical range of k_{600} estimates from days with higher GPP (Fig. 4a). Reasonable k_{600} estimates from days with $\bar{P}_{GPP}$ above the chosen threshold provided an approximately normal distribution with a mean of 0.145 m h^{-1} and a standard deviation of 0.023 m h^{-1} (Fig. 5). A normal model of the results of the dome experiments provided a distribution with a somewhat smaller mean, but with a much broader range of estimates that included the full range of the whole-reach parameter estimates at high GPP (mean of 0.119 m h^{-1} and standard deviation of 0.085 m h^{-1}). These values are similar to gas exchange velocities for reaches with slopes ranging from 0.0003 m to 0.005 m m^{-1} in downstream reaches of the Colorado River (Hall et al. 2012).

Using the prior distribution of k_{600} based on days with high GPP, the Eulerian dynamic flow model with the highest posterior probability generally provided reliable predictions of downstream DO dynamics, during both steady and unsteady flow conditions (e.g., Fig. 6). When using parameter values with the highest posterior probabilities, the model typically describes more than 99% of the total variance in downstream DO concentrations (i.e., $R^2 > 0.99$). Periods of poor performance in fitting the coupled model (as indicated by lower R^2 values) were typically attributable to atypical DO data, rather than obvious systematic problems with the model or parameter estimation approach (with the exception of the aforementioned interdependence of k_{600} and R_{ER}).

Comparison of dynamic and steady flow parameter estimates

When applied to steady flow conditions, differences in the daily metabolism estimates ($\bar{P}_{GPP}$ and $\bar{R}_{ER}$ with highest posterior probability) and model fits (R^2) were negligible between the Eulerian dynamic flow and Lagrangian steady flow model estimates (Fig. 7a,b). Additionally, the joint probability distributions of posterior probabilities for the daily metabolism estimates were indistinguishable (Fig. 8a).

When applied to unsteady flow conditions, the Eulerian dynamic flow model provided a better fit (R^2=0.994, Fig. 7c) relative to the Lagrangian steady flow model parameterized with the daily average velocity and depth (R^2=0.968, Fig. 7d). The steady flow model overestimated the magnitude of both GPP (10.5 g O_2 m^{-2} d^{-1} vs. 9.5 g O_2 m^{-2} d^{-1}) and ER (–11.8 g O_2 m^{-2} d^{-1} vs. −9.1 g O_2 m^{-2} d^{-1}) relative to estimates from the dynamic flow model (Fig. 7c,d). The joint probability distributions of posterior probabilities for the daily metabolism estimates had no meaningful overlap between the two models (Fig. 8b). Some skepticism should be maintained in drawing detailed conclusions from

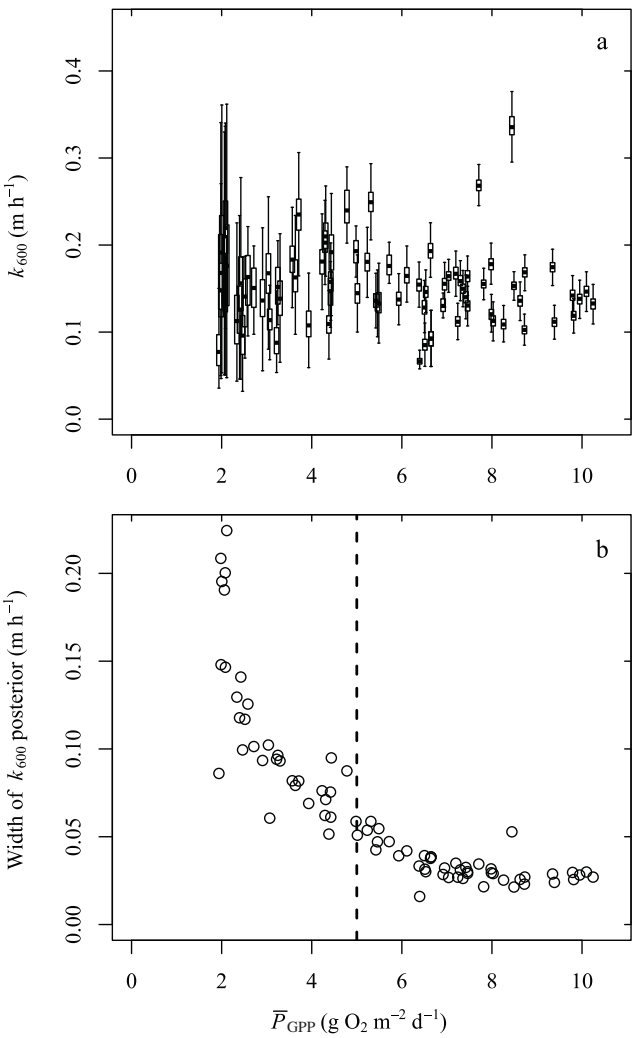

Fig. 4. (**a**) Posterior distributions of estimates of k_{600} over a period of consistent increase in GPP (07 January 2009–20 April 2009), plotted against $\bar{P}_{GPP}$. Box and whisker plots summarize the distributions as follows: center marks are the medians, boxes are the interquartile ranges, and whiskers extend to the 5th and 95th percentiles. (**b**) Width of the posterior distributions as characterized by the magnitude of the difference between the 5th and 95th percentiles. We interpret the width of the posterior distribution as an inverse index of confidence in k_{600} estimates based on the precision in the parameter estimate inferred from variation in DO data for a given day of analysis.

comparisons of the relative overlap of these posterior distributions of parameter estimates, because they do not account for all sources of error and parameter uncertainty is likely underestimated when based on a likelihood function that does not account for autocorrelation in error.

Discussion

We have introduced and provided initial assessments of a method for estimating whole river metabolism during unsteady flow conditions, based on coupling a hydrologic

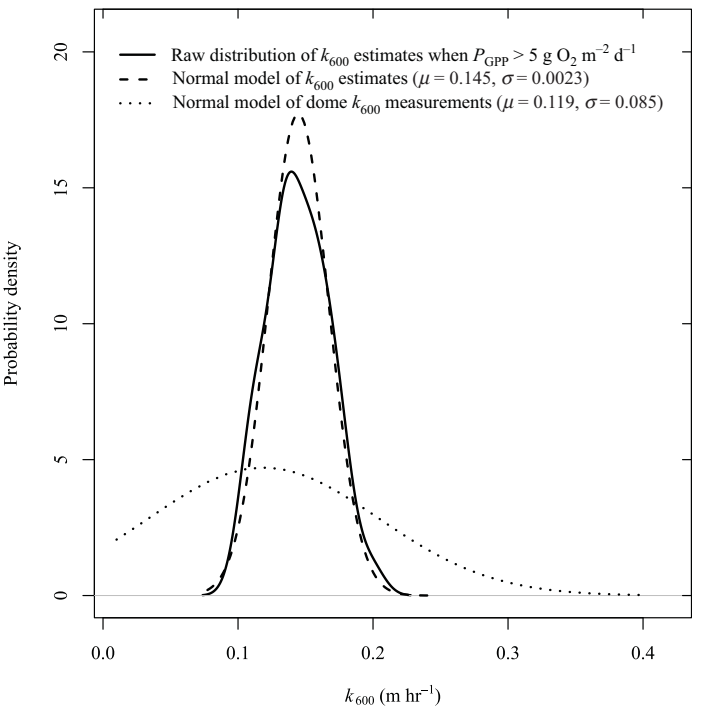

Fig. 5. Probability density functions for the raw distribution (solid line) and normal model (dashed line) for the population of reasonable highest posterior probability k_{600} estimates when $\bar{P}_{GPP}$ exceeds 5 g O$_2$ m^{-2} d^{-1} during the period of 07 January through 20 April 2009 (*see* Fig. 4). The normal model of the distribution of point estimates of k_{600} from dome experiments is provided (dotted line) for comparison.

flow routing model with an ecosystem metabolism model. Heuristics from the effort and subsequent model assessment allow us to comment on general aspects of integrated model development, as well as more specific aspects of hydrologic and metabolic modeling in rivers.

Integrated models in shared state space

This coupled modeling effort was facilitated by the use of a shared state-space system, specifically the framework provided by NEO (Izurieta et al. 2012). The key to model integration is a strategy for managing computational interdependencies where coupled models "overlap" in state space. For example, a critical overlap between the hydrologic and metabolic models for this effort was advection in the river flow edges (Fig. 1), where the hydrologic model predicts the flow of water and the metabolic model uses the flow state value to calculate the advection of DO. As a result of the ability to share states in NEO, integration of the metabolic model was relatively easy, compared to the remainder of the model and parameter estimation development effort. First, the hydrological model was already implemented and tested, so design of the metabolic model in the shared state space required no further hydrologic considerations. Second, the fundamental controls on state-space initialization, dependency tracking, and output monitoring were already

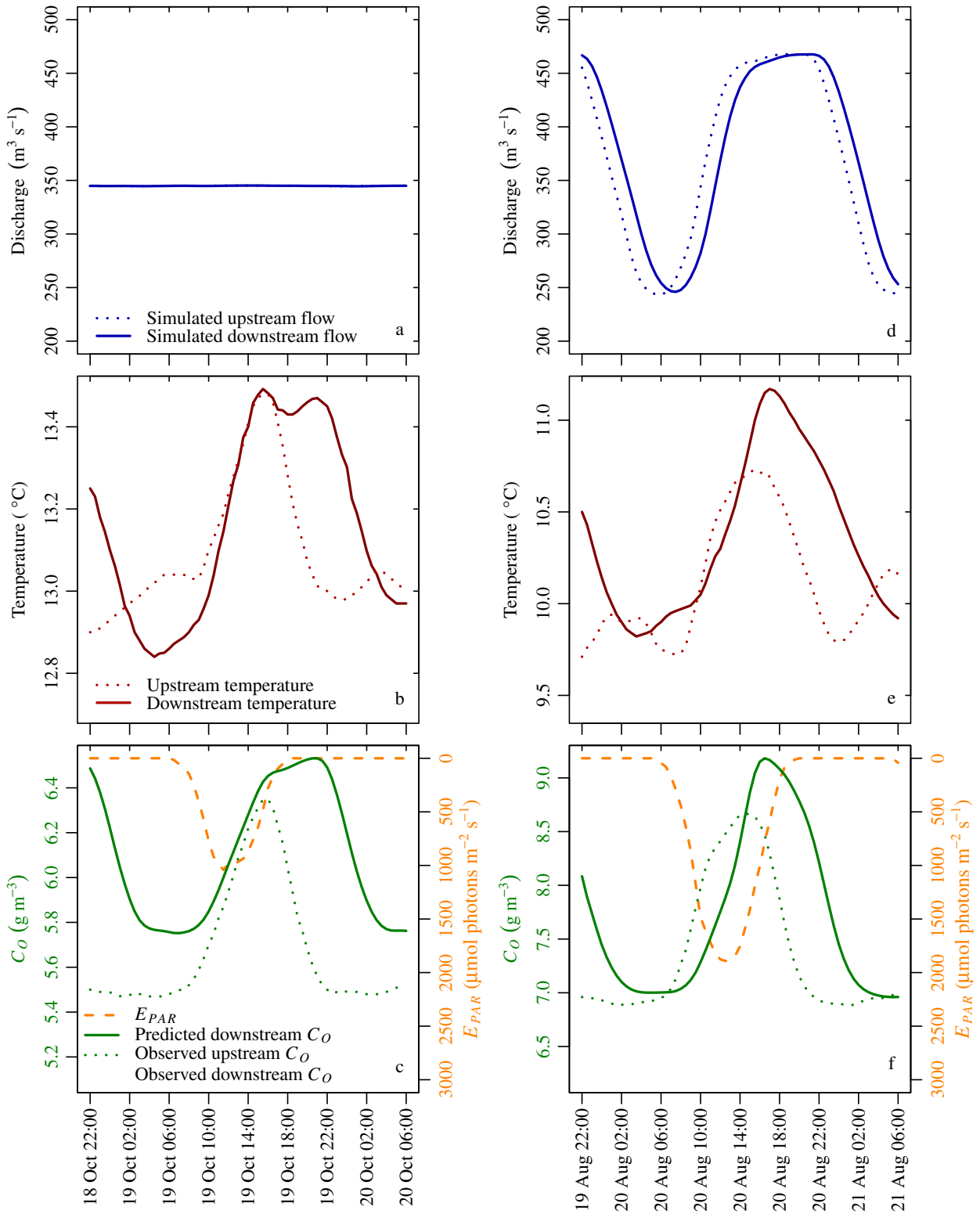

Fig. 6. Example of driving data and Eulerian dynamic flow model results from daily metabolic estimates for 19 October 2008 (steady flow) and 20 August 2010 (unsteady flow). (**a**, **d**) Simulated upstream (dotted line) and downstream (solid line) river discharges based on the calibrated hydrologic model. (**b**, **e**) Measured upstream (dotted line) and downstream (solid line) temperature from the water quality sondes. (**c**, **f**) Theoretical E_{PAR} (dashed orange line plotted on inverted scale), measured upstream (dotted green line) and downstream (green circles) DO concentrations, and highest posterior probability simulated downstream DO concentrations (green line). Parameter estimates for 19 October 2008 were $\bar{P}_{GPP}$=3.5 g O_2 m^{-2} d^{-1}, $\bar{R}_{ER}$=−6.2 g O_2 m^{-2} d^{-1}, and k_{600}=0.15 m h^{-1} (R^2=0.993). Parameter estimates for 20 August 2010 were $\bar{P}_{GPP}$=9.4 g O_2 m^{-2} d^{-1}, $\bar{R}_{ER}$=−8.7 g O_2 m^{-2} d^{-1}, and k_{600}=0.16 m h^{-1} (R^2=0.993).

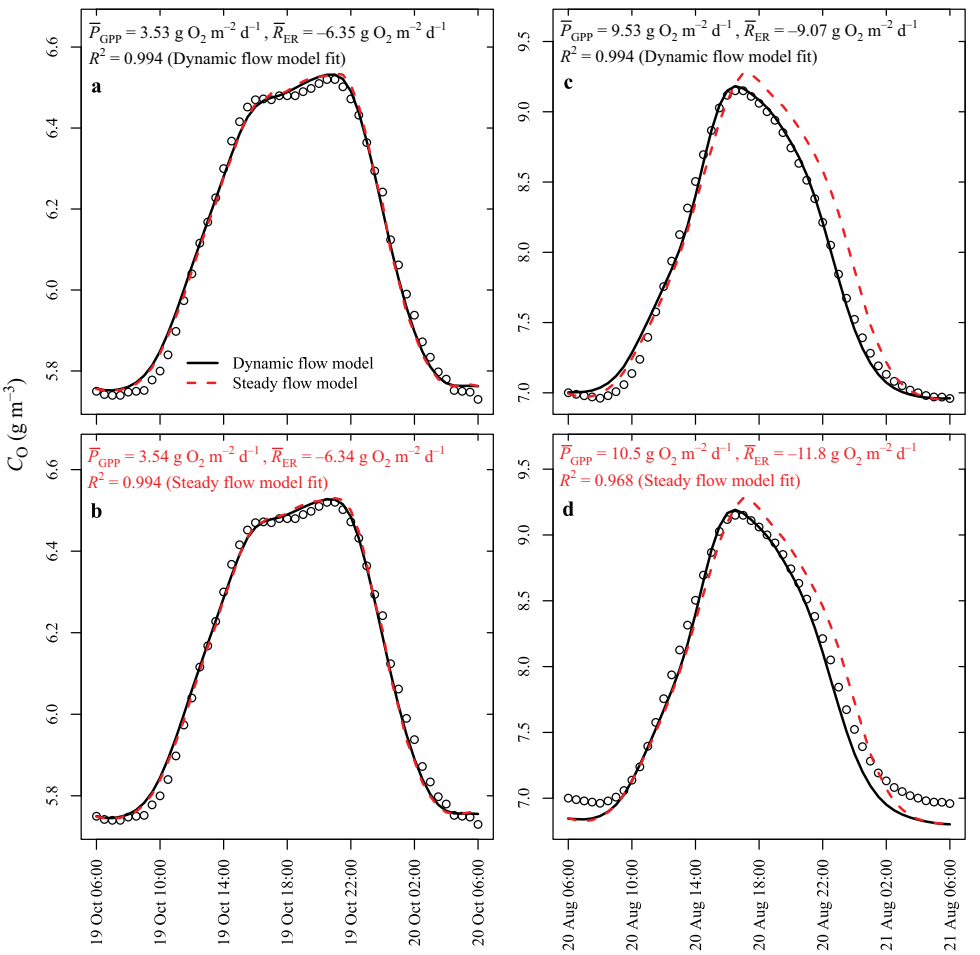

Fig. 7. Predictions (lines) and observations (points) of downstream DO concentrations based on the highest posterior probability metabolism parameter sets for (**a**, **b**) 19 October 2008, a day with steady flow and (**c**, **d**) 20 August 2010, a day with unsteady flow. All figures include output from both the Eulerian dynamic flow model (solid black line) and the Lagrangian steady flow model (dashed red line) executed with the best fit parameters associated with the respective figure. Figures in the first row (**a**, **c**) are model outputs based on parameter sets estimated using the Eulerian dynamic flow model. Figures in the second row (**b**, **d**) are model outputs based on parameters sets estimated using the Lagrangian steady flow model. Daily average GPP and ER estimates and R^2 of the respective model fits are provided at the top of each figure.

implemented in the NEO framework. In short, the implementation pathway from the conceptual model (Fig. 1) to a fully functional prototype was a matter of a few hours of coding work on a handful of Java classes. This efficiency allowed for more resources to be applied toward designing the tools for hydrologic and metabolic inferences from Bayesian statistics.

The inherent modularity and extensibility of a shared state-space framework also facilitates development of models for future efforts to explore some of the more problematic complications in estimation of whole river metabolic rates. For example, the module for simulation of respiration ("R_{ER} edge" in Fig. 1), is easily substitutable at run time with alternative conceptual models of the controls on respiration, such as those that can account for diel variation. The ability to substitute different complexities of ER simulations at run time is a valuable feature toward parsimonious model selection schemes, such as use of information criteria (e.g., Akaike Information Criterion (Akaike 1974)) or use of a Bayes Factor analysis (Marshall et al. 2005) that inherently rewards fit but penalizes complexity. Furthermore, an additional module may be implemented with states that track the isotopic ratios of DO, such that parameters controlling diel variation of ER can be estimated with the benefit of additional independent observations (Holtgrieve et al. 2010). Inclusion of this module in the simulation can be easily switched on or off, depending on whether isotopic data are available for analysis. Overall, this effort provides a straightforward illustration of the value of implementing environmental models in abstract, extensible frameworks with a shared state space.

Calibration of the hydraulic model

Our estimates of the friction parameters for Glen Canyon were substantially different from those estimated by Wiele

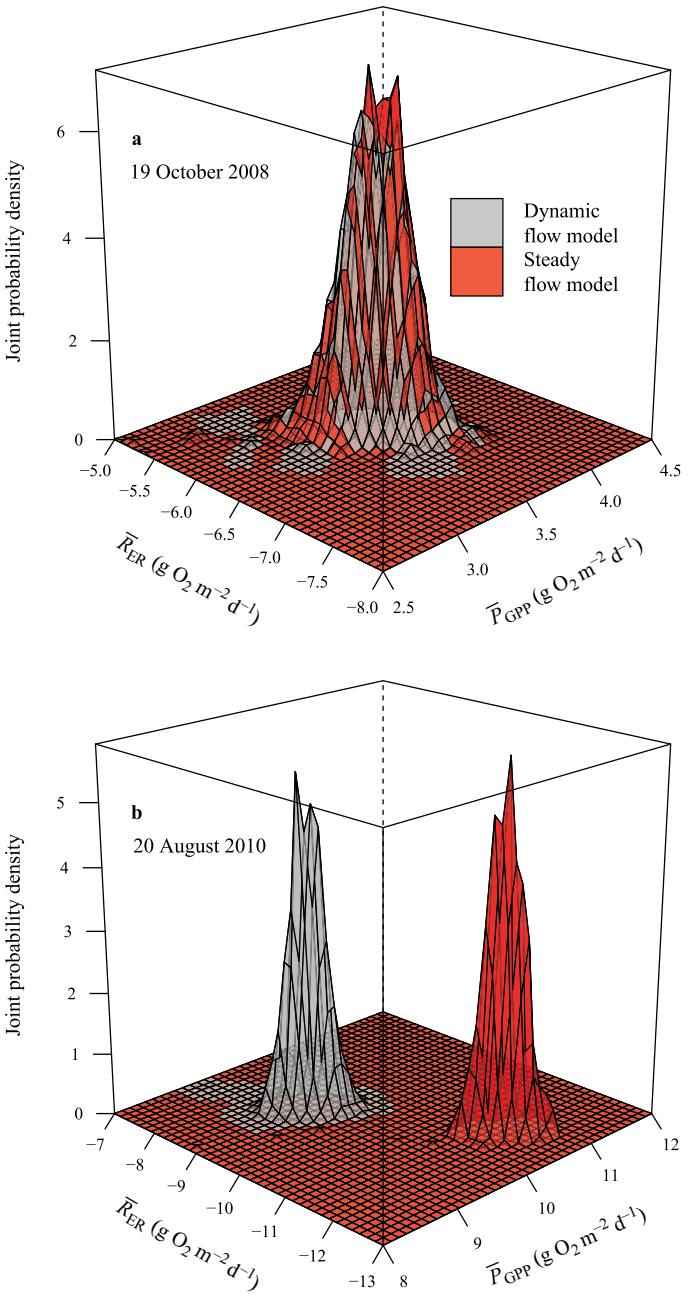

Fig. 8. Joint density of the posterior probability distributions for daily average $\bar{P}_{GPP}$ and $\bar{R}_{ER}$ on (**a**) 19 October 2008, a day with steady flow and (**b**) 20 August 2010, a day with unsteady flow. For each day, posterior distributions were estimated from Bayesian inference using both the Eulerian dynamic flow model (gray parameter surface) and the Lagrangian steady flow model (red parameter surface).

and Smith (1996) for a much longer section of the Colorado River below Glen Canyon Dam ($f_b = -5.544$ and $f_m = 5.104$). This disparity is not surprising, because we are working with a much shorter and geomorphically uniform reach compared to the longer reach of the previous study, and spatial variation in these parameters for isolated reaches in the region is likely to be substantial across major geomorphic discontinuities (e.g., among Glen Canyon, Marble Canyon, and the Grand Canyon proper).

In hydraulic model development, we found further support for the conclusions of Wiele and Smith (1996) that water depth has a strong influence on the effects of friction (i.e., Manning's roughness) along the Colorado River. The hydraulic model proved impossible to calibrate in initial attempts with a static value for Manning's roughness, either with a realistic value for the roughness coefficient or with a reasonable fit to flow and velocity data. This finding also supports the suggestion by Wiele and Smith (1996) that larger geomorphological elements (e.g., bedrock constriction or channel form variation) are more likely to control dynamics of channel water retention in Glen Canyon, because changes in discharge would be expected to have a lesser effect on retention where smaller channel elements (e.g., bed roughness or algae/plant communities) were the dominant controls on friction in a relatively deep river.

In performing this recalibration, we have demonstrated an effective method for calibrating hydraulic routing models, without direct comparison of simulations to hydrograph or velocity time series data (Figs. 2, 3). Calibration of a dynamic-wave routing model requires that predictions be compared to observations in terms of both the movement of mechanical energy (i.e., flood pulse celerity) and the movement of water (i.e., water and solute velocity) along the channel. By calibrating to the observed relationship between discharge and velocity, we were able to determine effective friction parameter values without a more complex multivariate likelihood function and without a detailed time series of reach average velocity.

While detailed time series of velocity data are not necessary, this calibration scheme does require a strategic sampling of reach average velocities and discharges over a range of flow conditions. Reach average velocity measurements should be collected at relatively evenly distributed flow states that span the full range of discharges experienced during the metabolism analysis period. Similar to standards for establishing discharge vs. depth rating curves for river gauges, this practice avoids the inherent uncertainties of extrapolation or interpolation in data-poor regions of the discharge vs. velocity calibration. Furthermore, the data set should include a comparable number of observations from periods when flow is increasing vs. decreasing, to avoid potential bias created by calibration to data that has oversampled the lower or upper side of flood pulse hystereses (Fig. 2).

Bayesian priors and the controls of GPP on gas exchange estimates

Use of informed prior probabilities in a Bayesian inference scheme may allow improved inferences of parameter values

that are likely to be confounded by parameter interactions (i.e., model equifinality). In this effort, we demonstrated how precision in inference of air–water gas exchange increases with the amplitude of daily variation in DO concentrations due to increases in GPP. This pattern resulted in a collection of days with higher precision in k_{600} estimates (i.e., more information about gas exchange in DO observations), from which we derived the prior distribution for all subsequent parameter estimates, including those at times of the year with less diel variation in DO (Figs. 4 and 5). Effectively, this approach is an extrapolation of a descriptive statistical model of higher-precision air-gas exchange rate estimates to periods of time when DO variation contains less unique information about k_{600}. As with all extrapolations, this method should be applied with careful consideration of the applicability of the prior distribution and careful communication of assumptions. However, it provides some hope in situations where detailed independent information about interacting parameters is simply unavailable, and it provides an example of the potential utility of informative priors in Bayesian inference (Hooten and Hobbs 2015).

In this work, we also showed that independent information about air–water gas exchange from dome experiments was relatively broad, but comparable to the prior distributions generated from whole-reach estimates during the higher-precision period (Fig. 5). The broader range of k_{600} estimates from the dome experiments indicate that point measurements of gas exchange may have been driven by a broader range of localized conditions, relative to the aggregated influences driving daily whole-reach estimates from Bayesian inference. However, whole-reach estimates and dome estimates also had relatively similar means with respect to the broader distribution of the dome estimates, suggesting that the use of dome estimates as prior information for Bayesian inference would not have meaningfully changed our estimates of k_{600} that were based on a uniform prior distribution. We interpret this relative pattern in independent dome data as corroborating evidence that daily whole-reach estimates of k_{600} at high GPP were a reasonable inference of the effects of gas exchange over the reach during the study period, and that the normal model for dome data may be equally defensible as a prior distribution to use for inference of gas exchange parameter values.

This approach is useful for data-limited scenarios, but does not completely resolve the known uncertainties in ER estimates stemming from uncertainties in air–water gas exchange or invalid assumptions about the time invariance of ER. In the end, we suggest our method is consistent with most approaches proposed for estimating metabolism in aquatic ecosystems, in that the estimates of ER are inherently less robust than those of GPP (McCutchan et al. 1998).

Comparison of the dynamic flow model with conventional models

Computational artifacts from differing model structures had little influence on estimates of metabolism between the dynamic and steady flow models, despite the known effects of numerical dispersion in Eulerian models relative to Lagrangian models. Each cell of the Eulerian model effectively mixes instantly during each time step, resulting in a solute transport effect identical to a purposeful simulation of longitudinal dispersion. The typical Lagrangian model used for metabolism estimates (including ours) does not share this dispersive character because there is no mixing among the conceptual parcels of water as they travel the reach.

Despite structural differences, the two models still agreed on metabolism estimates during steady flow, both in terms of the fit with highest posterior probability and the structure of posterior parameter distributions (Figs. 7a,b, 8a). Differences in the model structure are likely irrelevant to metabolism estimates because the temporal patterns in DO that provide information about metabolism have a much longer time scale than those that are affected by the numerical dispersion inherent in the Eulerian model. In other words, the Eulerian model effectively "smooths out" any higher-frequency (among minutes) noise that is present in the upstream DO measurements, but the more gradual changes in DO (among hours) attributable to metabolism are not affected by numerical dispersion in the model. The effects of numerical dispersion as a computational artifact should not be confused with the potential effects of real hydrodynamic dispersion on lower-frequency DO dynamics. Lack of consideration of mechanical dispersion in DO transport in models may still cause bias in metabolism estimates depending on the influence of dispersive transport relative to advective transport time (Hensley and Cohen 2016), but exploration of potential biases from this common simplification in river metabolic models are outside the scope of this study.

Because there are no apparent differences in metabolism estimates from the two models during steady flow conditions (Figs. 7a,b, 8a), we suggest that analysis with the Eulerian dynamic flow model is conceptually consistent with the extensive library of Lagrangian whole-stream metabolism methods derived from Odum's original approach (Odum 1956; Marzolf et al. 1994). On the other hand, differences between the two models during unsteady flow conditions (Figs. 7c,d, 8b) demonstrate the potential for substantial inconsistencies in metabolism estimates when variations in DO transport times are not considered relative to when they are simulated. Thus, we add "unsteady flow conditions" to the list of hydraulic considerations that are important for unbiased estimates of whole-river metabolism (Hensley and Cohen 2016). Finally, comparisons of the accuracy in predictions of downstream DO observations (Fig. 7c,d) suggest that the Eulerian dynamic flow is effective in simulating the influence of

variable transport times on metabolic processes, at least in comparison with the Lagrangian steady flow model.

Comments and recommendations

The development of new integrated environmental models is a pressing need in the effort to extract inferences and scientific insight from an exponentially growing pool of continuous time-series datasets. Our model construction effort is an example of how models designed to use a common state space can substantially facilitate the development of those coupled models. Another strategy is to design models that implement a standard information-sharing interface, allowing models built to use that interface to extract information from other models during runtime. Regardless of the specific strategy employed, we recommend that future model and inferential tool development efforts continue to show a similar level of consideration for extensibility in computational model structures, such that models can be coupled directly during runtime with fewer development resources allocated to software adaptation and redesign.

Using our approach, estimation of whole-stream metabolic rates under dynamic flow conditions first requires a dataset allowing simulation of the relationship between discharge and water velocity over the study reach. We demonstrated a method using natural variation in water quality, but additional calibration data for smaller streams can be obtained by repeating artificial conservative tracer releases under multiple flow conditions. If the natural variation of water quality can be modeled directly, then this approach may also be modified to calibrate directly to the discharge and water quality time-series data at the base of the study reach, thus removing potential for errors that may be introduced by fitting a line to hysteretic observations. Regardless of the approach, calibration of this model is not possible without some variant of reach-averaged velocity data, which are far less commonly available than discharge data.

This work also demonstrates useful generalizations regarding the inference of both air–water gas exchange rates and ecosystem respiration rates from the same DO dataset, regardless of whether the model is operated under dynamic or steady flow conditions. We suggest that periods of higher GPP provide less confounded estimates of air–water gas exchange rates, and comparisons of these more reliable rates with measured rates from independent experiments (if available) provide a useful quality assurance procedure when establishing a continuous metabolism gauging station. Furthermore, use of a Bayesian inference scheme with prior probabilities informed by high GPP data or independent measurements provides a means to help reduce the inherent confounding effects between estimates of physical gas exchange and respiration.

Data associated with figures in this paper will be publicly searchable and available from the U. S. Geological Survey ScienceBase repository (https://www.sciencebase.gov/catalog/, https://doi.org/10.5066/F76T0KG2).

APPENDIX

Summary of variables and details of physical dissolved gas calculations

Saturated DO concentration

Values of C_{OS} were calculated using theoretical relationships with water temperature, water density, and atmospheric

Table A1. Summary of variables. Variables in bold are parameters that were estimated by Bayesian inference.

Variable	Dimensions	Description
$\boldsymbol{\alpha_{GPP}}$	[M]	Proportionality constant for GPP vs. photosynthetically active radiation
θ	-	Proposed parameter set
ρ_w	[M L^{-3}]	Density of water
σ^2	varies	Variance of residual error
A	[L^2]	Cross-sectional area of the river channel
A_{WS}	[L^2]	Plan area of the channel water surface
C_O	[M L^{-3}]	Dissolved oxygen concentration
C_{OD}	[M L^{-3}]	Saturation deficit of dissolved oxygen
C_{OS}	[M L^{-3}]	Saturation concentration for dissolved oxygen
D_O	-	Observed data set
d_O	varies	Observed data point
d_P	varies	Predicted data point
E_{PAR}	[L^{-2} T^{-1}]	Photosynthetically active radiation energy
$\boldsymbol{f_b}$	-	Intercept of friction-depth model
$\boldsymbol{f_m}$	-	Logarithmic slope of friction-depth model
g	[L T^{-2}]	Acceleration due to gravity
H	[L]	Hydraulic head
J_O	[M L^{-2} T^{-1}]	Mass flux of oxygen due to air-water exchange

Table A1. Continued

Variable	Dimensions	Description
k	[L T^{-1}]	Gas exchange velocity for oxygen
$\boldsymbol{k}_{600}$	[L T^{-1}]	Gas exchange velocity at a Schmidt number of 600
M_O	[M]	Mass of dissolved oxygen
n	-	Manning's roughness coefficient
P_{GPP}	[M L^{-2} T^{-1}]	Instantaneous gross primary production flux
$\bar{P}_{GPP}$	[M L^{-2} T^{-1}]	Daily average gross primary production flux
p	[L]	Ambient barometric pressure
p_s	[L]	Standard atmospheric pressure
Q	[L^3 T^{-1}]	River discharge
Q_E	[L^3 T^{-1}]	Exchange of water between river cells due to flow
R	[L]	Hydraulic radius of the river channel
$\boldsymbol{R}_{\mathbf{ER}}$	[M L^{-2} T^{-1}]	Instantaneous ecosystem respiration
$\bar{R}_{ER}$	[M L^{-2} T^{-1}]	Daily average ecosystem respiration
S_0	[L L^{-1}]	Bed slope
S_C	-	Schmidt number
t	[T]	Time
t_D	[T]	Time a water parcel passes the downstream end of a reach
t_U	[T]	Time a water parcel passes the upstream end of a reach
$\bar{t}_R$	[T]	Reach average travel time
T	[Θ]	Temperature
$\bar{T}$	[Θ]	Reach average temperature
T_S	-	Normalized temperature index
u	[L T^{-1}]	Depth average velocity at a given river location
u^*	[L T^{-1}]	Shear velocity
V	[L^3]	Volume of water in a river cell
x	[L]	Longitudinal distance along the river
$\bar{z}$	[L]	Reach average river depth

pressure. The saturation concentration for oxygen in water at standard atmospheric pressure ($C_{OS,ATM}$, g m^{-3}) was calculated as an empirical function of temperature (García and Gordon 1992).

$$C_{OS,ATM} = 0.032\rho_w \exp(5.80871 + 3.20291T_S + 4.17887T_S^2 + 5.10006T_S^3 - 0.0986643T_S^4 + 3.80369T_S^5) \quad \text{(A1)}$$

where 0.032 is the molecular weight of O_2 (mg μmol^{-1}), ρ_w is the density of river water (kg L^{-1}), and T_S is a dimensionless normalized temperature index for river water. The exponential term in equation A1 is an empirical estimate of saturated oxygen concentration in units of μmol kg^{-1}. The value of T_S was calculated as a function of water temperature (García and Gordon 1992).

$$T_S = \ln\left(\frac{298.15 - T}{273.15 + T}\right) \quad \text{(A2)}$$

where T is the temperature of river water (°C). Water density was also calculated as an empirical function of water temperature.

$$\rho_w = 0.999842 + 6.7940\times10^{-5}T - 9.0953\times10^{-6}T^2 + 1.0017\times10^{-7}T^3 - 1.1201\times10^{-9}T^4 + 6.5363\times10^{-12}T^5 \quad \text{(A3)}$$

Values of $C_{OS,ATM}$ were adjusted for ambient barometric pressure based on Henry's Law.

$$C_{OS} = C_{OS,ATM}\frac{p}{p_S} \quad \text{(A4)}$$

where p is the ambient barometric pressure (mm Hg), and p_S is equal to standard atmospheric pressure (760 mm Hg). For the current study, we do not consider the influence of temporal variability in barometric pressure on DO exchange between the channel and atmosphere, and p is set to a constant 682 mm Hg based on elevation of the study reach. If future work finds this to be a significant source of error in metabolism estimates, then pressure can be changed to a time-variant model input and elevation-corrected values can be obtained from regional meteorological stations.

Schmidt number

The Schmidt number was calculated empirically (Wanninkhof 1992).

$$S_C = 1800.6 - 120.1T + 3.7818T^2 - 0.047608T^3 \quad \text{(A5)}$$

The temperature- and gas-dependent value of k was subsequently calculated from the temperature- and gas-independent exchange velocity at a Schmidt number of 600 (k_{600}, m s^{-1}) (Jähne et al. 1987).

$$k = k_{600}\left(\frac{S_C}{600}\right)^{-0.5} \quad \text{(A6)}$$

where k_{600} is a model parameter and is assumed constant for a given day of analysis.

References

Akaike, H. 1974. A new look at the statistical model identification. IEEE Trans. Automat. Contr. **19**: 716–723. doi:10.1109/TAC.1974.1100705

Bednarek, A. T., and D. D. Hart. 2005. Modifying dam operations to restore rivers: Ecological responses to Tennessee River dam mitigation. Ecol. Appl. **15**: 997–1008. doi:10.1890/04-0586

Cole, J. J., and others. 2007. Plumbing the global carbon cycle: Integrating inland waters into the terrestrial carbon budget. Ecosystems **10**: 171–184. doi:10.1007/s10021-006-9013-8

Cross, W. F., C. V. Baxter, K. C. Donner, E. J. Rosi-marshall, T. A. Kennedy, R. O. Hall, H. A. Wellard Kelly, and R. S. Rogers. 2011. Ecosystem ecology meets adaptive management: Food web response to a controlled flood on the Colorado River, Glen Canyon. Ecol. Appl. **21**: 2016–2033. doi:10.1890/10-1719.1

Cushman, R. M. 1985. Review of ecological effects of rapidly varying flows downstream from hydroelectric facilities. N. Am. J. Fish. Manag. **5**: 330–339. doi:10.1577/1548-8659(1985)5<330:ROEEOR>2.0.CO;2

Doyle, M. W., and S. H. Ensign. 2009. Alternative reference frames in river system science. Bioscience **59**: 499–510. doi:10.1525/bio.2009.59.6.8

Ensign, S. H., M. W. Doyle, and J. R. Gardner. 2017. New strategies for measuring rates of environmental processes in rivers, lakes, and estuaries. Freshwater Science **36**: 453–465. doi:10.1086/692998

García, H. E., and L. I. Gordon. 1992. Oxygen solubility in seawater: Better fitting equations. Limnol. Oceanogr. **37**: 1307–1312. doi:10.4319/lo.1992.37.6.1307

Grams, P. E., J. C. Schmidt, and D. J. Topping. 2007. The rate and pattern of bed incision and bank adjustment on the Colorado River in Glen Canyon downstream from Glen Canyon Dam, 1956–2000. Geol. Soc. Am. Bull. **119**: 556–575. doi:10.1130/B25969.1

Hall, R. O., T. A. Kennedy, and E. J. Rosi-Marshall. 2012. Air–water oxygen exchange in a large whitewater river. Limnol. Oceanogr. Fluids Environ. **2**: 1–11. doi:10.1215/21573689-1572535

Hall, R. O., C. B. Yackulic, T. A. Kennedy, M. D. Yard, E. J. Rosi-Marshall, N. Voichick, and K. E. Behn. 2015. Turbidity, light, temperature, and hydropeaking control primary productivity in the Colorado River, Grand Canyon. Limnol. Oceanogr. **60**: 512–526. doi:10.1002/lno.10031

Hall, R. O., J. L. Tank, M. A. Baker, E. J. Rosi-Marshall, and E. R. Hotchkiss. 2016. Metabolism, gas exchange, and carbon spiraling in rivers. Ecosystems **19**: 73–86. doi:10.1007/s10021-015-9918-1

Helton, A. M., G. C. Poole, R. A. Payn, C. Izurieta, and J. A. Stanford. 2014. Relative influences of the river channel, floodplain surface, and alluvial aquifer on simulated hydrologic residence time in a montane river floodplain. Geomorphology **205**: 17–26. doi:10.1016/j.geomorph.2012.01.004

Hensley, R. T., and M. J. Cohen. 2016. On the emergence of diel solute signals in flowing waters. Water Resour. Res. **52**: 759–772. doi:10.1002/2015WR017895

Holtgrieve, G. W., D. E. Schindler, T. A. Branch, and Z. T. A'mar. 2010. Simultaneous quantification of aquatic ecosystem metabolism and reaeration using a Bayesian statistical model of oxygen dynamics. Limnol. Oceanogr. **55**: 1047–1062. doi:10.4319/lo.2010.55.3.1047

Hooten, M. B., and N. T. Hobbs. 2015. A guide to Bayesian model selection for ecologists. Ecol. Monogr. **85**: 3–28. doi:10.1890/07-1861.1

Hotchkiss, E. R., and R. O. Hall. 2014. High rates of daytime respiration in three streams: Use of $\delta^{18}O\text{-}O_2$ and O_2 to model diel ecosystem metabolism. Limnol. Oceanogr. **59**: 798–810. doi:10.4319/lo.2014.59.3.0798

Hotchkiss, E. R., R. O. Hall, R. A. Sponseller, D. Butman, J. Klaminder, H. Laudon, M. Rosvall, and J. Karlsson. 2015. Sources of and processes controlling CO_2 emissions change with the size of streams and rivers. Nat. Geosci. **8**: 696–699. doi:10.1038/ngeo2507

Izurieta, C., G. C. Poole, R. A. Payn, I. Griffith, R. Nix, A. M. Helton, E. S. Bernhardt, and A. J. Burgin. 2012. Development and application of a simulation environment (NEO) for integrating empirical and computational investigations of system-level complexity. *In* Proceedings of International Conference on Information Science and Applications. doi:10.1109/ICISA.2012.6220928

Jähne, B., K. O. Münnich, R. Bösinger, A. Dutzi, H. Werner, and P. Libner. 1987. On the parameters influencing air-water gas exchange. J. Geophys. Res. **92**: 1937–1949. doi:10.1029/JC092iC02p01937

Kennedy, T. A., and others. 2016. Flow management for hydropower extirpates aquatic insects, undermining river food webs. Bioscience **66**: 561–575. doi:10.1093/biosci/biw059

Marino, R., and R. W. Howarth. 1993. Atmospheric oxygen exchange in the Hudson River: Dome measurements and comparison with other natural waters. Estuaries **16**: 433–445. doi:10.2307/1352591

Marshall, L., D. Nott, and A. Sharma. 2004. A comparative study of Markov chain Monte Carlo methods for

conceptual rainfall-runoff modeling. Water Resour. Res. **40**: W02501. doi:10.1029/2003WR002378

Marshall, L. A., D. Nott, and A. Sharma. 2005. Hydrological model selection: A Bayesian alternative. Water Resour. Res. **41**: W10422. doi:10.1029/2004WR003719

Marzolf, E. R., P. J. Mulholland, and A. D. Steinman. 1994. Improvements to the diurnal upstream-downstream dissolved oxygen change technique for determining whole-stream metabolism in small streams. Can. J. Fish. Aquat. Sci. **51**: 1591–1599. doi:10.1139/f94-158

McCutchan, J. H., W. M. Lewis, Jr., and J. F. Saunders, III. 1998. Uncertainty in the estimation of stream metabolism from open-channel oxygen concentrations. J. North Am. Benthol. Soc. **17**: 155–164. doi:10.2307/1467959

Melis, T. S., J. Korman, and T. A. Kennedy. 2012. Abiotic and biotic responses of the Colorado River to controlled floods at Glen Canyon Dam, Arizona, USA. River Res. Appl. **28**: 764–776. doi:10.1002/rra.1503

Mulholland, P. J., and others. 2001. Inter-biome comparison of factors controlling stream metabolism. Freshw. Biol. **46**: 1503–1517. doi:10.1046/j.1365-2427.2001.00773.x

Odum, H. T. 1956. Primary production in flowing waters. Limnol. Oceanogr. **1**: 102–117. doi:10.4319/lo.1956.1.2.0102

Poff, N. L., J. D. Allan, M. B. Bain, J. R. Karr, K. L. Prestegaard, B. D. Richter, R. E. Sparks, and J. C. Stromberg. 1997. The Natural Flow Regime: A paradigm for river conservation and restoration. Bioscience **47**: 769–784. doi:10.2307/1313099

Poole, G. C., J. A. Stanford, S. W. Running, C. A. Frissell, W. W. Woessner, and B. K. Ellis. 2004. A patch hierarchy approach to modeling surface and subsurface hydrology in complex flood-plain environments. Earth Surf. Process. Landforms **29**: 1259–1274. doi:10.1002/esp.1091

Raymond, P. A., and others. 2013. Global carbon dioxide emissions from inland waters. Nature **503**: 355–359. doi:10.1038/nature12760

Rossman, L. A. 2006. Storm water management model quality assurance report: Dynamic wave flow routing. Report EPA/600/R-06/097. US Environmental Protection Agency. Cincinnati, OH.

Smith, T. J., and L. A. Marshall. 2008. Bayesian methods in hydrologic modeling: A study of recent advancements in Markov chain Monte Carlo techniques. Water Resour. Res. **44**: W00B05. doi:10.1029/2007WR006705

Tobias, C. R., J. K. Böhlke, and J. W. Harvey. 2007. The oxygen-18 isotope approach for measuring aquatic metabolism in high-productivity waters. Limnol. Oceanogr. **52**: 1439–1453. doi:10.4319/lo.2007.52.4.1439

Topping, D. J., and others. 2010. Sediment transport during three controlled-flood experiments on the Colorado River downstream from Glen Canyon Dam, with implications for eddy-sidebar deposition in Grand Canyon National Park. Open-File Report 2010–1128. U. S. Geological Survey. Reston, VA.

Walton, R., T. H. Martin, Jr., R. S. Chapman, and J. E. Davis. 1995. Investigation of wetlands hydraulic and hydrological processes, model development, and application. Wetland Program Technical Report WRP-CP-6. US Army Corps of Engineers. Washington, DC.

Wanninkhof, R. 1992. Relationship between wind speed and gas exchange over the ocean. J. Geophys. Res. **97**: 7373–7382. doi:10.1029/92JC00188

Wiele, S. M., and J. D. Smith. 1996. A reach-averaged model of diurnal discharge wave propagation down the Colorado River through the Grand Canyon. Water Resour. Res. **32**: 1375–1386. doi:10.1029/96WR00199

Williamson, C. E., W. K. Dodds, T. K. Kratz, and M. A. Palmer. 2008. Lakes and streams as sentinels of environmental change in terrestrial and atmospheric processes. Front. Ecol. Environ. **6**: 247–254. doi:10.1890/070140

Yard, M. D., G. E. Bennett, S. N. Mietz, L. G. Coggins, L. E. Stevens, S. Hueftle, and D. W. Blinn. 2005. Influence of topographic complexity on solar insolation estimates for the Colorado River, Grand Canyon, AZ. Ecol. Modell. **183**: 157–172. doi:10.1016/j.ecolmodel.2004.07.027

Zimmerman, J. K. H., B. H. Letcher, K. H. Nislow, K. A. Lutz, and F. J. Magilligan. 2010. Determining the effects of dams on subdaily variation in river flows at a whole-basin scale. River Res. Appl. **26**: 1246–1260. doi:10.1002/rra.1324

Acknowledgments

We thank Tyler Smith for source code critical to implementing the Bayesian inference software, and we thank Adam Copp for collection and organization of field data. We thank the editors, anonymous reviewers, Charles Yackulic, and Scott Wright for their comments that helped improve the clarity of this manuscript. Funding for this study was provided by the U. S. Department of the Interior Bureau of Reclamation's Glen Canyon Dam Adaptive Management Program via a cooperative agreement among the U. S. Geological Survey, Montana State University, and the University of Wyoming (agreement #G10AC00141). This work was also supported by the National Science Foundation EPSCoR Cooperative Agreement #EPS-1101342 via the Montana Institute on Ecosystems. Any use of trade, firm, or product names is for descriptive purposes only and does not imply endorsement by the U.S. Government.

Conflict of Interest

None declared.

Submitted 22 February 2017
Revised 28 June 2017
Accepted 25 July 2017

Associate editor: Gordon Holtgrieve